A simple genetic basis for managing maternally transmitted symbionts

Lisa J. Funkhouser-Jones[1,2,6*], Edward J. van Opstal[1,6*], Ananya Sharma[1] and Seth R. Bordenstein[1,3,4,5,7*]

[1] Department of Biological Sciences, Vanderbilt University, Nashville, TN 37235, USA.

[2] Department of Molecular Microbiology, Washington University School of Medicine in St. Louis, Saint Louis, MO 63110, USA.

[3] Department of Pathology, Microbiology, and Immunology, Vanderbilt University, Nashville, TN 37235, USA.

[4] Vanderbilt Institute for Infection, Immunology and Inflammation, Vanderbilt University, Nashville, TN 37235, USA.

[5] Vanderbilt Genetics Institute, Nashville, TN 37235, USA.

[6] These authors contributed equally to this work.

[7] Lead contact

* Corresponding authors. Email: s.bordenstein@vanderbilt.edu (SRB), lisa.j.funkhouser@gmail.com (LJF), edward.j.van.opstal@vanderbilt.edu (EjvO)

SUMMARY

Maternal transmission of intracellular microbes is pivotal in establishing long-term, intimate symbioses. For germline microbes that exert negative reproductive effects on their hosts, selection can theoretically favor the spread of host genes that counteract the microbe's harmful effects. Here, we leverage a major difference in bacterial (*Wolbachia pipientis*) titers between closely-related wasp species with forward genetic, transcriptomic, and cytological approaches to map two quantitative trait loci that suppress bacterial titers via a maternal effect. Fine mapping and knockdown experiments identify the gene *Wolbachia density suppressor* (*Wds*), which dominantly suppresses bacterial transmission from mother to embryo. *Wds* evolved by lineage-specific amino acid changes driven by positive selection. Collectively, our findings demonstrate that a genetically simple change arose by Darwinian selection in less than a million years to regulate maternally transmitted bacteria via a dominant, maternal effect gene.

INTRODUCTION

All animals harbor microbial communities that participate in beneficial processes [1] as diverse as nutritional uptake and metabolism [2, 3], immune cell development [4-6], and pathogen resistance [7, 8]. However, even innocuous microbes can become harmful when not properly regulated [9, 10], and intracellular microbes that are transmitted over multiple host generations can have negative fitness effects on their hosts [11-13]. In these intimate and enduring germline symbioses, hosts are predicted to evolve suppression that reduces the harmful effects of the symbiont [14-16]. However, little is known about the genes and evolutionary forces that underpin regulation of maternally-transmitted symbionts despite the repeated and independent origins of maternal transmission in diverse host taxa [17]. Reverse genetic studies in insects suggest immune or developmental genes may evolve to affect endosymbiont densities [18-21] but, to our knowledge, no studies have utilized forward genetic approaches to characterize the gene(s) underlying variation in host regulation of maternally-transmitted symbionts.

Here, we utilize a major host interspecific difference in titers of the maternally-transmitted bacteria *Wolbachia* and quantitative trait loci analyses to identify a suppressor gene in the emerging *Nasonia* model. *Nasonia* (Order: Hymenoptera) is a genus of parasitoid wasps comprised of four closely-related species, with *N. vitripennis* last sharing a common ancestor with the other three species approximately one million years ago [22, 23]. In the lab, interspecific crosses of *Nasonia* species produce viable and fertile hybrid females, which permits the transfer of genetic or cytoplasmic material (including intracellular *Wolbachia*) between *Nasonia* species. Consequently, *Nasonia* is a powerful model system for studying the quantitative genetics of interspecific variation in host traits such as wing size [24-26], head shape [27], sex pheromones [28, 29], and memory retention [30].

Nasonia species are all naturally infected with different *Wolbachia* strains, mostly acquired through horizontal transfer after species divergence [31]. *Wolbachia* (Order Rickettsiales) are vertically-transmitted, intracellular bacteria that infect 40-52% of all arthropod species [32, 33]. In most insects, including in *Nasonia*, *Wolbachia* are reproductive parasites that manipulate host reproduction through a variety of mechanisms to achieve a greater proportion of females in the host population [34, 35]. Both efficient transovarial transmission and host reproductive manipulation by the parasite often depend upon sufficiently high within-host *Wolbachia* densities [36, 37]; however, overproliferation of *Wolbachia* can drastically reduce lifespan in *Drosophila* [13, 38], mosquitoes [39, 40] and terrestrial isopods [41]. Thus, coadaptation between arthropod hosts and *Wolbachia* strain(s) can promote genetic and phenotypic changes that impact transmission of *Wolbachia* densities [42-47]. When co-adapted host and symbiont pairs are disrupted through experimental transfer of *Wolbachia* into a naïve host, control of the symbiosis is often lost, leading to overproliferation, expanded tissue tropism of *Wolbachia*, and/or fitness costs not witnessed in the original host species [41, 47-49].

Transfer of a specific *Wolbachia* strain (*w*VitA) from one *Nasonia* species (*N. vitripennis*) to a naïve, closely-related species (*N. giraulti*) results in a major perturbation in which the relative *Wolbachia* load increases by two orders of magnitude with an associated reduction in fecundity [47]. Importantly, *w*VitA densities and *Nasonia* fecundity return to normal when *w*VitA is crossed back into a *N. vitripennis* genomic background from the high-density *N. giraulti* line (IntG). Since both the native *N. vitripennis* and the *w*VitA-infected *N. giraulti* IntG lines have the same cytotype, the interspecific *Wolbachia* density variation is established by variation in the host nuclear genome [47]. In this study, we utilize several forward genetic techniques in *Nasonia* to dissect the genetic, evolutionary, and cytological basis of maternal regulation of *Wolbachia*. The varied approaches

77 culminate in the characterization of two quantitative trait loci and the discovery of *Wolbachia*
78 *density suppressor (Wds)*, a positively-selected, maternal effect gene that suppresses the
79 transmission of *Wolbachia*.
80
81 **RESULTS**
82 ***Nasonia vitripennis* dominantly suppresses *w*VitA titers through a maternal genetic effect**
83 To determine the inheritance pattern of *w*VitA densities, we reciprocally crossed *N.*
84 *vitripennis* (low-density) and *N. giraulti* IntG (high-density) individuals and measured the
85 *Wolbachia* densities of F1 female hybrids using quantitative PCR (qPCR) for a single-copy
86 *Wolbachia* gene (*groEL*) normalized to a *Nasonia* gene (*NvS6K*) (Figure 1A). The average F1
87 female pupal *Wolbachia* densities from pure-breeding *N. vitripennis* (N = 5) and *N. giraulti* control
88 families (N = 5) were 0.057 ± 0.004 and 4.805 ± 1.071 (mean ± S.E.M.), respectively, which
89 represents an 84-fold interspecific difference in *Wolbachia* titers and is consistent with previous
90 studies [47]. Interestingly, while F1 hybrid females from both crosses had identical genotypes (i.e.,
91 heterozygous at all loci) and cytotypes (*N. vitripennis*), the average *Wolbachia* densities in
92 reciprocal F1 hybrid females were significantly different at 0.149 ± 0.029 vs 1.746 ± 0.187 (Figure
93 1A, N = 10 for both crosses, Kruskal-Wallis test: $H = 24.99$, $df = 3$, $p < 0.0001$, Dunn's multiple
94 comparisons test: $p = 0.03$).
95 To test whether the difference in F1 *Wolbachia* densities was due to maternal *Wolbachia*
96 load or to a maternal genetic effect, we backcrossed F1 females to their paternal line and pooled
97 five female F2 pupae per F1 mother for qPCR (Figure 1B). If a maternal genetic effect regulates
98 *Wolbachia* densities, F2 pupae from both experimental lines should have similar *Wolbachia* levels
99 since F1 hybrid mothers are genotypically identical. Indeed, the densities of F2 pupal offspring of
100 both high- and low-density F1 mothers (F2-2 and F2-1, respectively) were not significantly

different (Figure 1B, 0.161 ± 0.024, N = 13 and 0.086 ± 0.007, N = 14, respectively, Dunn's multiple comparisons test: p = 0.18), supporting the inference that maternal nuclear genotype plays an important role in regulating *Wolbachia* densities. Furthermore, since the densities of both F2 hybrid groups were more similar to the *N. vitripennis* control (0.053 ± 0.001, N = 6) than to the *N. girault*i control (3.364 ± 0.174, N = 6), the *N. vitripennis* low *Wolbachia* density phenotype is dominant (Figure 1B).

Disparities in embryonic *w*VitA levels between *N. vitripennis* and *N. girault*i are established during oogenesis

We previously showed that variation in *w*VitA loads between *N. vitripennis* and *N. girault*i IntG exists in early embryos, with strict posterior localization of *w*VitA in *N. vitripennis* that is perturbed in *N. girault*i IntG embryos [47]. Since the *w*VitA density disparity is partially controlled through a maternal genetic effect (Figure 1B), we reasoned that an embryonic disparity in *w*VitA densities between *N. vitripennis* and *N. girault*i is likely established in the egg chamber during oogenesis (Figure 1C). Indeed, nucleic acid staining with SYTOX Green revealed that fewer *w*VitA cells are present in stage three *N. vitripennis* egg chambers (Figure 1D) than in *N. girault*i oocytes at the same stage (Figure 1E). Furthermore, *w*VitA cells in *N. vitripennis* are distributed equally between the oocyte and nurse cells (Figure 1D), whereas most *w*VitA cells in *N. girault*i egg chambers are present in the oocyte (Figure 1E). Once in the oocyte, *w*VitA localizes exclusively to the posterior pole in *N. vitripennis* (Figure 1D), but has an expanded distribution toward the anterior end of the oocyte in *N. girault*i (Figure 1E). Importantly, the lack of puncta in ovaries from uninfected *N. vitripennis* confirms that the SYTOX nucleic acid dye effectively stains *Wolbachia* but no other cytoplasmic elements, such as mitochondria (Figure 1F). Altogether, the

distribution and density of *w*VitA in oocytes of these two *Nasonia* species perfectly mirror their embryonic *w*VitA patterns [47], suggesting that *Wolbachia* density differences are established during oogenesis and regulated through maternal-effect genes, rather than zygotic genes expressed later in embryonic development.

Phenotype-based selection and introgression identifies two maternal suppressor genomic regions

In an initial approach to determine the location and number of loci that suppress *w*VitA densities in *N. vitripennis*, we selected upon the dominant, low-density phenotype of this species while serially backcrossing hybrid females to *N. giraulti* IntG males (Figure 2A). Since the phenotype is controlled through a maternal genetic effect, hybrid females were selected based on the *w*VitA densities of their offspring, with sisters of the low-density offspring used as mothers in the next round of introgression (Figure 2A). Two independent selection lines were generated simultaneously to help discriminate between *N. vitripennis* regions maintained due to selection (present in both lines) versus those maintained through chance (present in only one line).

For each independent line, DNA from three females that produced ninth-generation offspring with the lowest *Wolbachia* densities were pooled and genotyped on a *Nasonia* genotyping microarray composed of 19,681 sequence markers that differ between *N. vitripennis* and *N. giraulti* [50]. Both selection lines (Lines 1 and 2) displayed an enrichment of *N. vitripennis* alleles along the central portions of chromosomes 2 and 3 (Figure 2B) out of *Nasonia*'s five chromosomes. On the most recent *N. vitripennis* linkage map [50], the area of enrichment on chromosome 2 for Line 1 occurs between 38 cM and 51.1 cM, while enrichment in Line 2 extends from 25.6 cM to 38 cM (Figure 2B). Although overlap in *N. vitripennis* allele enrichment between

147 Lines 1 and 2 on chromosome 2 occurs at 38 cM, the exact position and size of the overlap cannot
148 be determined due to the fact that it falls within the poorly-assembled heterochromatic regions
149 flanking the centromere [50]. For chromosome 3, the areas of enrichment for *N. vitripennis* alleles
150 between Lines 1 and 2 coincide starting at 35 cM and ending at 47.5 cM.
151
152 **QTL analysis validates the two maternal effect suppressor regions**
153 To validate the *Wolbachia* density-suppressing chromosomal regions determined through
154 phenotypic selection, we performed an independent quantitative trait loci (QTL) analysis in which
155 F1 hybrid females were backcrossed to high-density *N. giraulti* (IntG) males to obtain 191 F2
156 recombinant females. Each F2 female was phenotyped by measuring the *Wolbachia* densities of
157 her F3 pupal offspring. Since the most informative individuals in QTL mapping are those with the
158 most extreme phenotypes [51], we selectively genotyped F2 females with the lowest (0.072 –
159 0.409, N = 42) and highest (2.958 – 10.674, N = 42) F3 pupal *Wolbachia* titers with a total of 47
160 microsatellite markers across chromosomes 1, 2 and 3 with an average distance between markers
161 of 3 cM (Table S1). Using genotype data for selected individuals and phenotype data for all F2
162 females (Data S1), we identified two significant QTL regions at a genome-wide significance level
163 of $\alpha = 0.05$ (LOD > 2.29): one QTL peak on chromosome 2 at 43 cM ($p < 0.001$) and the other on
164 chromosome 3 at 41.5 cM ($p < 0.001$) (Figure 2C). Strikingly, the 95% Bayes credible interval on
165 chromosome 2 corresponds to the same region identified by the genotyping microarray as enriched
166 for *N. vitripennis* alleles in introgression Line 1 (38 cM – 51.1 cM), while the 95% Bayes credible
167 interval on chromosome 3 also contains a region that was enriched for *N. vitripennis* alleles (35
168 cM – 47.5 cM) in both introgression lines. Thus, the microarray and QTL analyses complement

each other and confirm that suppressor genes of major effect for *w*VitA density are located near the centromeric regions on chromosomes 2 and 3.

As a negative control, we genotyped the same individuals with markers located on *Nasonia* chromosome 1 (Data S1), which was not enriched for *N. vitripennis* alleles after the selection introgression. In the QTL analysis, the highest peak on chromosome 1 was not statistically significant (Figure 2C), indicating again that chromosomes 2 and 3 are likely the only chromosomes harboring genes of major effect for the *w*VitA density trait.

To determine the effect of each QTL on density suppression, the average percent reduction in F3 pupal *Wolbachia* densities was calculated for the F2 females with *N. vitripennis* alleles at markers close to one or both of the calculated QTL peaks. Females with an *N. vitripennis* allele on the chromosome 2 or chromosome 3 QTLs produced offspring with a 52% or 32% reduction in densities, respectively, compared to offspring of females that were homozygous *N. giraulti* at both QTL loci (Figure 2C, inset). Furthermore, these effects acted additively for a 91% reduction in densities in offspring of females with *N. vitripennis* alleles at both loci compared to offspring of F2 females with *N. giraulti* alleles at both loci (Figure 2C, inset).

Marker-assisted introgression confirms and narrows the maternal effect suppressor QTL on chromosome 3

To validate the QTLs on chromosomes 2 and 3 and narrow the gene candidate regions, we independently introgressed the QTL regions from *N. vitripennis* into an *N. giraulti* IntG background for at least nine generations using marker-assisted selection (similar to Figure 2A, see Materials and Methods). After the ninth generation, we conducted sibling matings to produce segmental introgression lines that were homozygous *N. vitripennis* for the marker of interest.

Unfortunately, generating *N. vitripennis* homozygous lines for the chromosome 2 region was not possible due to hybrid sterility, so we focused exclusively on the chromosome 3 region.

The initial homozygous and heterozygous introgression lines generated from sibling matings identified a candidate region 3.4 Mb in size containing 288 genes (Line IntC3) that suppressed *w*VitA densities by 60%, while lines lacking this region had little to no density suppression (Figure 3, Data S2). Surprisingly, the percent effect of the chromosome 3 homozygous introgression on *Wolbachia* suppression was nearly double that observed in the QTL study (60% vs 32%, Figure 2C inset). However, the QTL study was performed on F2 hybrid females while the introgression lines underwent at least nine generations of backcrossing. If there was an *N. vitripennis*-specific negative regulator of the *Wolbachia* suppressor gene on a different chromosome, then the allele would likely be present in F2 hybrids but would have recombined out with subsequent backcrossing to *N. giraulti* IntG. The stronger phenotype could also be due to the homozygous introgression lines having two copies of the *N. vitripennis* chromosome 3 candidate region, while F2 hybrid females were heterozygous. However, this is unlikely since heterozygous introgression females had the same level of *Wolbachia* suppression as their homozygous counterparts (Fig. 3, C3-3 and C3-4 vs. C3-5 and C3-6, Kruskal-Wallis test: $H = 1.39$, $df = 3$, $p = 0.71$).

IntC3 was further backcrossed to IntG to generate four recombinant lines (R3, R4, R5, and R6) that suppressed *w*VitA densities by 58 – 78% (depending on the line) with an overlapping candidate region of 780 kb and 44 genes (Fig. 3). Finally, R6 was backcrossed to IntG to obtain three recombinant lines, two of which caused 67% (R6-2) and 68% (R6-3) density suppression. The overlapping *N. vitripennis* region in the R6-2 and R6-3 lines was 165 kb and contained only 32 genes (Figure 3).

215

216 **RNA-seq identifies a single candidate gene (*Wds*) based on expression differences in**

217 ***Nasonia* ovaries**

218 To identify candidate genes within the 165 kb, 32-gene region that are differentially

219 expressed in the maternal germline of *N. vitripennis* and *N. giraulti*, we performed high-throughput

220 RNA sequencing (RNA-seq) on four independent pools of 40 ovary samples from the parental *N.*

221 *vitripennis* 12.1 strain and the IntC3 line from the first round of introgressions as well as five

222 independent pools from the *N. giraulti* IntG line (Table S2). Seven genes in the 32-gene candidate

223 region exhibited significant differences in expression between the three aforementioned lines

224 (Table S3). However, since the density trait is controlled through a dominant *N. vitripennis*

225 maternal effect (Figure 1B), we reasoned that the most likely candidate gene(s) would be

226 upregulated in *N. vitripennis* compared to *N. giraulti*. Only one of the seven genes

227 (*LOC100679092*) was consistently and significantly overexpressed in *N. vitripennis* and IntC3

228 (low density) compared to IntG (high density). Thus, we focused on *LOC100679092* for further

229 analysis. As an uncharacterized gene with no known protein domains, we hereby name the gene

230 *Wds* for *Wolbachia density suppressor* gene. Overexpression of *Wds* in ovaries of *N. vitripennis*

231 and IntC3 compared to IntG was validated using RT-qPCR (79- and 92-fold, respectively, Figure

232 S1) in independent, biological replicates of the RNA-seq samples.

233

234 ***Wds* controls embryonic *w*VitA densities**

235 Several studies have successfully used parental RNAi in *Nasonia* to examine the effects of

236 maternal genes on embryonic development [52-57]. If the *N. vitripennis* allele of *Wds* (Wds_v) is

237 responsible for suppressing *Wolbachia* titers, we expect that post-transcriptional knockdown of

238 *Wds*$_v$ transcripts in IntC3 mothers will result in less density suppression and, consequently, an
239 increase in *w*VitA levels in the resulting embryos. Indeed, injection of IntC3 mothers with dsRNA
240 against *Wds*$_v$ significantly increased offspring embryonic *w*VitA densities (696 ± 67.9, N = 24) by
241 56% or 63% compared to embryonic *w*VitA densities from mothers injected with dsRNA against
242 a control bacterial gene, maltose transporter subunit E (*MalE*) (447 ± 52.1, N = 24) or buffer-
243 injected females (426 ± 50.3, N = 23), respectively (Figure 4A, Kruskal-Wallis test: H = 13.1, df
244 = 3, $p < 0.01$, Dunn's multiple comparisons test: $p = 0.006$ and $p = 0.027$ compared to control *Wds*$_v$
245 group). This increase coincided with a 57% knock-down in *Wds*$_v$ gene expression in RNAi females
246 compared to the buffer-injected controls (Figure 4B, Mann Whitney U test, $p = 0.0015$).
247 Furthermore, we compared embryonic *w*VitA densities from mothers injected with dsRNA against
248 *Nasonia* gene LOC100679394 (*Mucin-5AC*), a gene that was significantly upregulated in *N.*
249 *vitripennis* but immediately outside the chromosome 3 candidate region. Embryos from mothers
250 injected with dsRNA against *Mucin-5AC* did not produce significantly higher *w*VitA densities
251 (459 ± 75.9, N = 25) compared to embryos from either *MalE*-RNAi (447 ± 52.1, N = 24) or buffer-
252 injected females (426 ± 50.3, N = 25, Figure 4A), even though *Mucin-5AC*-RNAi mothers had a
253 71% decrease in *Mucin-5AC* gene expression versus buffer-injected controls (Figure S2, Mann
254 Whitney U test $p = 0.0003$).

255 To further validate the effect of *Wds*$_v$ on *Wolbachia* densities, R6-3 recombinant females
256 (homozygous *N. vitripennis* for the 32-gene candidate region only) were injected with dsRNA
257 against *Wds*$_v$. Knock-down of *Wds*$_v$ in females again significantly increased embryonic *w*VitA
258 densities (314 ± 34.4, N = 21) by 43% or 54% compared to embryonic *w*VitA densities from
259 mothers injected with dsRNA against the control bacterial gene *MalE* (219 ± 39.2, N = 19) or from
260 buffer-injected females (204 ± 28.4, N = 20), respectively (Figure 4C, Mann Whitney U, $p = 0.049$

and p = 0.023 compared to control Wds_v group). This increase coincided with a 45% knock-down in Wds_v gene expression in RNAi females compared to the buffer-injected controls (Figure 4D, Mann Whitney U test, p = 0.0041).

Wds undergoes accelerated evolution and positive selection

The *Nasonia* genus is comprised of four closely-related species, with *N. vitripennis* sharing a common ancestor with the other three species approximately one million years ago [22, 23]. Wds protein sequences are 95% identical between *N. vitripennis* and *N. giraulti* with ten amino acid differences (and no indels) out of 201 total amino acids (Figure S3). Between the more closely-related *N. giraulti* and *N. longicornis* species that diverged approximately 400,000 years ago [22], Wds is 99% identical with two amino acid differences that evolved specifically in *N. giraulti* (Figure S3). Interestingly, Wds in *Trichomalopsis sarcophagae*, the wasp species most closely-related to *Nasonia*, [58], shares 95% amino acid identity to the *N. vitripennis* protein, but 97% and 98% identity to the *N. giraulti* and *N. longicornis* proteins, respectively (Figure S3). The accelerated protein sequence evolution in *N. vitripennis* is driven by seven unique amino acid changes that differ from conserved residues present in all three other homologs (Figure 5A, Figure S3) [22]. Furthermore, three of those seven amino acid changes fall within a region of high positive selection based on a sliding window analysis of the Ka/Ks ratio (Figure 5B) [59]. Additionally, the isoelectric point (pI) of the Wds protein, an important factor in protein evolution [60], drops from 9.24 in *N. vitripennis* to 8.75 in *N. giraulti*. In contrast, the isoelectric point difference for the Mucin-5AC control is minimal (ΔpI = 0.04).

Overall, Wds in the *N. vitripennis* lineage experienced recent amino acid substitutions, perhaps in response to acquisition of the *w*VitA *Wolbachia* strain that horizontally transferred into

284 *N. vitripennis* after *N. vitripennis'* divergence from its common ancestor with *N. giraulti* and *N.*
285 *longicornis* [31]. Outside of these four species, the next closest orthologs of Wds are found in
286 wasps such as *Trichogramma pretiosum, Copidosoma floridanum*, and *Polistes canadensis*, but
287 they only share 29% – 42% amino acid identity to Wds_v across a majority of the sequence (Table
288 S4). While more distant orthologs are present in other Hymenopterans such as bees and ants (Table
289 S4), only portions of the proteins can be properly aligned. Thus, this work demonstrates rapidly
290 evolving, taxon-restricted genes can contribute directly to the adaptive evolution of regulating
291 maternal symbiont transmission.

DISCUSSION

The main goal of this study was to determine the number and types of animal gene(s) that control the intracellular abundance of a widespread, maternally-transmitted symbiont. Unlike reverse genetics screens that mutate genes and then look for phenotypes, which may reflect off-target effects of the mutation rather than the true function of the protein, the forward genetic screens deployed here utilized an unbiased, candidate-blind approach to reveal the simple, genetic basis of variation in host regulation of maternally-transmitted *Wolbachia*. The identification of the *Wds* gene demonstrates that host regulation of symbiont loads is adaptive and can proceed through lineage-specific amino acid changes in a maternal effect gene. The Wds protein has areas of low complexity and a predicted signal peptide at its N-terminus (Figure 5B), but it does not contain any characterized protein domains that elude to its function. Because *w*VitA bacteria are predominantly found in the oocytes of *N. giraulti* IntG (Figure 2D) but are equally present in the nurse cells and the oocytes of *N. vitripennis* (Figure 2E), we propose that the *Wds* maternal effect that establishes the density difference operates on *w*VitA trafficking between nurse cells and the oocyte in *Nasonia*. Though all *Wolbachia* in *Drosophila* egg chambers are transferred from the nurse cells to the oocyte during cytoplasmic dumping immediately prior to egg-laying [61], *Wolbachia* in *Nasonia* nurse cells appear to be excluded from the oocyte at the end of oogenesis (P. Ferree, personal communication). Thus, the *N. vitripennis Wds* allele could function as a molecular inhibitor or physical barrier that impedes *w*VitA trafficking from nurse cells to the oocyte, thereby suppressing *Wolbachia* loads in the resulting embryo. Furthermore, in *Drosophila*, *Wolbachia w*Mel cells in the oocyte increase proportionally faster than those in the nurse cells [61], which suggests that the high *w*VitA densities in *N. giraulti* could be a combination of

315 unrestrained shuttling of *w*VitA from the nurse cells into the oocyte as well as faster proliferation
316 of *w*VitA once in the oocyte.

317 The findings presented here indicate that keeping maternally-transmitted symbionts in
318 check can have a simple genetic basis, even for obligate intracellular bacteria that must be
319 regulated within host cells and tissues. Two genomic regions act additively to explain nearly all of
320 the two-order-magnitude difference in *w*VitA densities between *Nasonia* wasp species. Moreover,
321 a single maternal effect gene with a major consequence on the density phenotype demonstrates
322 how natural selection can rapidly shape the evolution of density suppression of maternally
323 transmitted symbionts in invertebrates.

ACKNOWLEDGMENTS

We would like to thank John Colbourne for his assistance with the *Nasonia* genotyping microarray, Jürgen Gadau for his helpful advice on QTL mapping, Jack Werren for providing the *Nasonia* genetic map before its publication, and Patrick Ferree for sharing his unpublished data of *Wolbachia* staining in *Nasonia* ovaries. We would also like to acknowledge Jeff Jones for helping with the MatLab heat-map figure. This work was supported by National Science Foundation award 1456778 to SRB and Graduate Research Fellowship 0909667 to LJF, National Institutes of Health awards (NIH) R01 AI132581 and R21 HD086833 to SRB, T32 GM008554, and a Vanderbilt Microbiome Initiative Award. Imaging was performed through the use of the Vanderbilt Cell Imaging Shared Resource (supported by NIH grants CA68485, DK20593, DK58404, DK59637 and EY08126). The funders had no role in study design, data collection and analysis, decision to publish, or preparation of the manuscript.

AUTHOR CONTRIBUTIONS

Conceptualization, L.J.F., E.J.vO, and S.R.B.; Methodology, L.J.F., E.J.vO, and S.R.B.; Formal Analysis, L.J.F. and E.J.vO; Investigation, L.J.F., E.J.vO, and A.S.; Writing – Original Draft, L.J.F. and E.J.vO; Writing – Review and Editing, L.J.F., E.J.vO, A.S., and S.R.B.; Visualization, L.J.F. and E.J.vO. Project Administration, S.R.B.; Funding Acquisition, L.J.F. and S.R.B.

DECLARATION OF INTERESTS

The authors declare no competing interests.

345 **REFERENCES**

346 1. McFall-Ngai, M., Hadfield, M.G., Bosch, T.C., Carey, H.V., Domazet-Loso, T., Douglas,
347 A.E., Dubilier, N., Eberl, G., Fukami, T., Gilbert, S.F., et al. (2013). Animals in a bacterial world,
348 a new imperative for the life sciences. Proc Natl Acad Sci U S A *110*, 3229-3236.

349 2. Ley, R.E., Turnbaugh, P.J., Klein, S., and Gordon, J.I. (2006). Microbial ecology: human
350 gut microbes associated with obesity. Nature *444*, 1022-1023.

351 3. Turnbaugh, P.J., Ley, R.E., Mahowald, M.A., Magrini, V., Mardis, E.R., and Gordon, J.I.
352 (2006). An obesity-associated gut microbiome with increased capacity for energy harvest. Nature
353 *444*, 1027-1031.

354 4. Round, J.L., Lee, S.M., Li, J., Tran, G., Jabri, B., Chatila, T.A., and Mazmanian, S.K.
355 (2011). The Toll-like receptor 2 pathway establishes colonization by a commensal of the human
356 microbiota. Science *332*, 974-977.

357 5. Ivanov, II, Frutos Rde, L., Manel, N., Yoshinaga, K., Rifkin, D.B., Sartor, R.B., Finlay,
358 B.B., and Littman, D.R. (2008). Specific microbiota direct the differentiation of IL-17-producing
359 T-helper cells in the mucosa of the small intestine. Cell Host Microbe *4*, 337-349.

360 6. Ivanov, II, Atarashi, K., Manel, N., Brodie, E.L., Shima, T., Karaoz, U., Wei, D., Goldfarb,
361 K.C., Santee, C.A., Lynch, S.V., et al. (2009). Induction of intestinal Th17 cells by segmented
362 filamentous bacteria. Cell *139*, 485-498.

363 7. Candela, M., Perna, F., Carnevali, P., Vitali, B., Ciati, R., Gionchetti, P., Rizzello, F.,
364 Campieri, M., and Brigidi, P. (2008). Interaction of probiotic Lactobacillus and Bifidobacterium
365 strains with human intestinal epithelial cells: adhesion properties, competition against
366 enteropathogens and modulation of IL-8 production. Int J Food Microbiol *125*, 286-292.

8. Fukuda, S., Toh, H., Hase, K., Oshima, K., Nakanishi, Y., Yoshimura, K., Tobe, T., Clarke, J.M., Topping, D.L., Suzuki, T., et al. (2011). Bifidobacteria can protect from enteropathogenic infection through production of acetate. Nature *469*, 543-547.

9. Calderone, R.A., and Fonzi, W.A. (2001). Virulence factors of Candida albicans. Trends Microbiol *9*, 327-335.

10. Mitchell, J. (2011). Streptococcus mitis: walking the line between commensalism and pathogenesis. Mol Oral Microbiol *26*, 89-98.

11. Perrot-Minnot, M.J., Cheval, B., Migeon, A., and Navajas, M. (2002). Contrasting effects of *Wolbachia* on cytoplasmic incompatability and fecundity in the haplodiploid mite *Tetranychus urticae*. Journal of Evolutionary Biology *15*, 808-817.

12. Fleury, F., Vavre, F., Ris, N., Fouillet, P., and Bouletreau, M. (2000). Physiological cost induced by the maternally-transmitted endosymbiont Wolbachia in the Drosophila parasitoid Leptopilina heterotoma. Parasitology *121 Pt 5*, 493-500.

13. Min, K.T., and Benzer, S. (1997). Wolbachia, normally a symbiont of Drosophila, can be virulent, causing degeneration and early death. Proc Natl Acad Sci U S A *94*, 10792-10796.

14. Koehncke, A., Telschow, A., Werren, J.H., and Hammerstein, P. (2009). Life and death of an influential passenger: Wolbachia and the evolution of CI-modifiers by their hosts. PLoS One *4*, e4425.

15. Hornett, E.A., Charlat, S., Duplouy, A.M., Davies, N., Roderick, G.K., Wedell, N., and Hurst, G.D. (2006). Evolution of male-killer suppression in a natural population. PLoS Biol *4*, e283.

16. Jaenike, J. (2009). Coupled population dynamics of endosymbionts within and between hosts. Oikos *118*, 353-362.

17. Funkhouser, L.J., and Bordenstein, S.R. (2013). Mom knows best: the universality of maternal microbial transmission. PLoS Biol *11*, e1001631.

18. Wang, J., Wu, Y., Yang, G., and Aksoy, S. (2009). Interactions between mutualist Wigglesworthia and tsetse peptidoglycan recognition protein (PGRP-LB) influence trypanosome transmission. Proc Natl Acad Sci U S A *106*, 12133-12138.

19. Login, F.H., Balmand, S., Vallier, A., Vincent-Monegat, C., Vigneron, A., Weiss-Gayet, M., Rochat, D., and Heddi, A. (2011). Antimicrobial peptides keep insect endosymbionts under control. Science *334*, 362-365.

20. Serbus, L.R., Ferreccio, A., Zhukova, M., McMorris, C.L., Kiseleva, E., and Sullivan, W. (2011). A feedback loop between Wolbachia and the Drosophila gurken mRNP complex influences Wolbachia titer. J Cell Sci *124*, 4299-4308.

21. Newton, I.L., Savytskyy, O., and Sheehan, K.B. (2015). Wolbachia utilize host actin for efficient maternal transmission in Drosophila melanogaster. PLoS pathogens *11*, e1004798.

22. Campbell, B.C., Steffen-Campbell, J.D., and Werren, J.H. (1993). Phylogeny of the Nasonia species complex (Hymenoptera: Pteromalidae) inferred from an internal transcribed spacer (ITS2) and 28S rDNA sequences. Insect molecular biology *2*, 225-237.

23. Raychoudhury, R., Desjardins, C.A., Buellesbach, J., Loehlin, D.W., Grillenberger, B.K., Beukeboom, L., Schmitt, T., and Werren, J.H. (2010). Behavioral and genetic characteristics of a new species of Nasonia. Heredity *104*, 278-288.

24. Gadau, J., Page, R.E., and Werren, J.H. (2002). The genetic basis of the interspecific differences in wing size in Nasonia (Hymenoptera; Pteromalidae): major quantitative trait loci and epistasis. Genetics *161*, 673-684.

412 25. Loehlin, D.W., Enders, L.S., and Werren, J.H. (2010). Evolution of sex-specific wing
413 shape at the widerwing locus in four species of Nasonia. Heredity *104*, 260-269.
414 26. Loehlin, D.W., Oliveira, D.C., Edwards, R., Giebel, J.D., Clark, M.E., Cattani, M.V., van
415 de Zande, L., Verhulst, E.C., Beukeboom, L.W., Munoz-Torres, M., et al. (2010). Non-coding
416 changes cause sex-specific wing size differences between closely related species of Nasonia. PLoS
417 genetics *6*, e1000821.
418 27. Werren, J.H., Cohen, L.B., Gadau, J., Ponce, R., Baudry, E., and Lynch, J.A. (2015).
419 Dissection of the complex genetic basis of craniofacial anomalies using haploid genetics and
420 interspecies hybrids in Nasonia wasps. Dev Biol.
421 28. Niehuis, O., Bullesbach, J., Judson, A.K., Schmitt, T., and Gadau, J. (2011). Genetics of
422 cuticular hydrocarbon differences between males of the parasitoid wasps Nasonia giraulti and
423 Nasonia vitripennis. Heredity *107*, 61-70.
424 29. Niehuis, O., Buellesbach, J., Gibson, J.D., Pothmann, D., Hanner, C., Mutti, N.S., Judson,
425 A.K., Gadau, J., Ruther, J., and Schmitt, T. (2013). Behavioural and genetic analyses of Nasonia
426 shed light on the evolution of sex pheromones. Nature *494*, 345-348.
427 30. Hoedjes, K.M., Smid, H.M., Vet, L.E., and Werren, J.H. (2014). Introgression study
428 reveals two quantitative trait loci involved in interspecific variation in memory retention among
429 Nasonia wasp species. Heredity (Edinb) *113*, 542-550.
430 31. Raychoudhury, R., Baldo, L., Oliveira, D.C., and Werren, J.H. (2009). Modes of
431 acquisition of Wolbachia: horizontal transfer, hybrid introgression, and codivergence in the
432 Nasonia species complex. Evolution *63*, 165-183.
433 32. Zug, R., and Hammerstein, P. (2012). Still a host of hosts for Wolbachia: analysis of recent
434 data suggests that 40% of terrestrial arthropod species are infected. PLoS One *7*, e38544.

435 33. Weinert, L.A., Araujo-Jnr, E.V., Ahmed, M.Z., and Welch, J.J. (2015). The incidence of
436 bacterial endosymbionts in terrestrial arthropods. Proc Biol Sci *282*, 20150249.
437 34. Werren, J.H., Baldo, L., and Clark, M.E. (2008). Wolbachia: master manipulators of
438 invertebrate biology. Nat Rev Microbiol *6*, 741-751.
439 35. Serbus, L.R., Casper-Lindley, C., Landmann, F., and Sullivan, W. (2008). The genetics
440 and cell biology of Wolbachia-host interactions. Annual review of genetics *42*, 683-707.
441 36. Perrot-Minnot, M.J., and Werren, J.H. (1999). *Wolbachia* infection and incompatibility
442 dynamics in experimental selection lines. J Evol Biol *12*, 272-282.
443 37. Dyer, K.A., Minhas, M.S., and Jaenike, J. (2005). Expression and modulation of embryonic
444 male-killing in Drosophila innubila: opportunities for multilevel selection. Evolution *59*, 838-848.
445 38. McGraw, E.A., Merritt, D.J., Droller, J.N., and O'Neill, S.L. (2002). Wolbachia density
446 and virulence attenuation after transfer into a novel host. Proc Natl Acad Sci U S A *99*, 2918-2923.
447 39. McMeniman, C.J., Lane, R.V., Cass, B.N., Fong, A.W., Sidhu, M., Wang, Y.F., and
448 O'Neill, S.L. (2009). Stable introduction of a life-shortening Wolbachia infection into the mosquito
449 Aedes aegypti. Science *323*, 141-144.
450 40. Suh, E., Mercer, D.R., Fu, Y., and Dobson, S.L. (2009). Pathogenicity of life-shortening
451 Wolbachia in Aedes albopictus after transfer from Drosophila melanogaster. Applied and
452 environmental microbiology *75*, 7783-7788.
453 41. Le Clec'h, W., Braquart-Varnier, C., Raimond, M., Ferdy, J.B., Bouchon, D., and Sicard,
454 M. (2012). High virulence of Wolbachia after host switching: when autophagy hurts. PLoS
455 pathogens *8*, e1002844.

456 42. Kim, J.K., Kim, N.H., Jang, H.A., Kikuchi, Y., Kim, C.H., Fukatsu, T., and Lee, B.L.
457 (2013). Specific midgut region controlling the symbiont population in an insect-microbe gut
458 symbiotic association. Applied and environmental microbiology *79*, 7229-7233.
459 43. Login, F.H., and Heddi, A. (2013). Insect immune system maintains long-term resident
460 bacteria through a local response. J Insect Physiol *59*, 232-239.
461 44. Mouton, L., Henri, H., Bouletreau, M., and Vavre, F. (2003). Strain-specific regulation of
462 intracellular Wolbachia density in multiply infected insects. Molecular ecology *12*, 3459-3465.
463 45. Kondo, N., Shimada, M., and Fukatsu, T. (2005). Infection density of Wolbachia
464 endosymbiont affected by co-infection and host genotype. Biology letters *1*, 488-491.
465 46. Rio, R.V., Wu, Y.N., Filardo, G., and Aksoy, S. (2006). Dynamics of multiple symbiont
466 density regulation during host development: tsetse fly and its microbial flora. Proc Biol Sci *273*,
467 805-814.
468 47. Chafee, M.E., Zecher, C.N., Gourley, M.L., Schmidt, V.T., Chen, J.H., Bordenstein, S.R.,
469 and Clark, M.E. (2011). Decoupling of host-symbiont-phage coadaptations following transfer
470 between insect species. Genetics *187*, 203-215.
471 48. Bian, G., Zhou, G., Lu, P., and Xi, Z. (2013). Replacing a native Wolbachia with a novel
472 strain results in an increase in endosymbiont load and resistance to dengue virus in a mosquito
473 vector. PLoS Negl Trop Dis *7*, e2250.
474 49. Le Clec'h, W., Raimond, M., Guillot, S., Bouchon, D., and Sicard, M. (2013). Horizontal
475 transfers of feminizing versus non-feminizing Wolbachia strains: from harmless passengers to
476 pathogens. Environ Microbiol.

50. Desjardins, C.A., Gadau, J., Lopez, J.A., Niehuis, O., Avery, A.R., Loehlin, D.W., Richards, S., Colbourne, J.K., and Werren, J.H. (2013). Fine-scale mapping of the Nasonia genome to chromosomes using a high-density genotyping microarray. G3 *3*, 205-215.

51. Lander, E.S., and Botstein, D. (1989). Mapping mendelian factors underlying quantitative traits using RFLP linkage maps. Genetics *121*, 185-199.

52. Lynch, J.A., Brent, A.E., Leaf, D.S., Pultz, M.A., and Desplan, C. (2006). Localized maternal orthodenticle patterns anterior and posterior in the long germ wasp Nasonia. Nature *439*, 728-732.

53. Lynch, J.A., Olesnicky, E.C., and Desplan, C. (2006). Regulation and function of tailless in the long germ wasp Nasonia vitripennis. Dev Genes Evol *216*, 493-498.

54. Ozuak, O., Buchta, T., Roth, S., and Lynch, J.A. (2014). Dorsoventral polarity of the Nasonia embryo primarily relies on a BMP gradient formed without input from Toll. Curr Biol *24*, 2393-2398.

55. Ozuak, O., Buchta, T., Roth, S., and Lynch, J.A. (2014). Ancient and diverged TGF-beta signaling components in Nasonia vitripennis. Dev Genes Evol *224*, 223-233.

56. Lynch, J.A., and Desplan, C. (2010). Novel modes of localization and function of nanos in the wasp Nasonia. Development *137*, 3813-3821.

57. Verhulst, E.C., Beukeboom, L.W., and van de Zande, L. (2010). Maternal control of haplodiploid sex determination in the wasp Nasonia. Science *328*, 620-623.

58. Werren, J.H., and Loehlin, D.W. (2009). The parasitoid wasp Nasonia: an emerging model system with haploid male genetics. Cold Spring Harb Protoc *2009*, pdb emo134.

498 59. Liang, H., Zhou, W., and Landweber, L.F. (2006). SWAKK: a web server for detecting
499 positive selection in proteins using a sliding window substitution rate analysis. Nucleic Acids Res
500 *34*, W382-384.
501 60. Alende, N., Nielsen, J.E., Shields, D.C., and Khaldi, N. (2011). Evolution of the isoelectric
502 point of mammalian proteins as a consequence of indels and adaptive evolution. Proteins *79*, 1635-
503 1648.
504 61. Ferree, P.M., Frydman, H.M., Li, J.M., Cao, J., Wieschaus, E., and Sullivan, W. (2005).
505 Wolbachia utilizes host microtubules and Dynein for anterior localization in the Drosophila
506 oocyte. PLoS pathogens *1*, e14.
507 62. Bordenstein, S.R., Marshall, M.L., Fry, A.J., Kim, U., and Wernegreen, J.J. (2006). The
508 tripartite associations between bacteriophage, Wolbachia, and arthropods. PLoS pathogens *2*, e43.
509 63. Bordenstein, S.R., and Bordenstein, S.R. (2011). Temperature affects the tripartite
510 interactions between bacteriophage WO, Wolbachia, and cytoplasmic incompatibility. PLoS One
511 *6*, e29106.
512 64. Broman, K.W., Wu, H., Sen, S., and Churchill, G.A. (2003). R/qtl: QTL mapping in
513 experimental crosses. Bioinformatics *19*, 889-890.
514 65. Robinson, M.D., McCarthy, D.J., and Smyth, G.K. (2010). edgeR: a Bioconductor package
515 for differential expression analysis of digital gene expression data. Bioinformatics *26*, 139-140.
516 66. Livak, K.J., and Schmittgen, T.D. (2001). Analysis of relative gene expression data using
517 real-time quantitative PCR and the 2(-Delta Delta C(T)) Method. Methods *25*, 402-408.
518 67. Pultz, M.A., Westendorf, L., Gale, S.D., Hawkins, K., Lynch, J., Pitt, J.N., Reeves, N.L.,
519 Yao, J.C., Small, S., Desplan, C., et al. (2005). A major role for zygotic hunchback in patterning
520 the Nasonia embryo. Development *132*, 3705-3715.

521 68. Kumar, S., Stecher, G., and Tamura, K. (2016). MEGA7: Molecular Evolutionary Genetics
522 Analysis Version 7.0 for Bigger Datasets. Mol Biol Evol *33*, 1870-1874.
523 69. Guindon, S., Dufayard, J.F., Lefort, V., Anisimova, M., Hordijk, W., and Gascuel, O.
524 (2010). New algorithms and methods to estimate maximum-likelihood phylogenies: assessing the
525 performance of PhyML 3.0. Syst Biol *59*, 307-321.
526 70. Huelsenbeck, J.P., and Ronquist, F. (2001). MRBAYES: Bayesian inference of
527 phylogenetic trees. Bioinformatics *17*, 754-755.
528 71. Letunic, I., and Bork, P. (2017). 20 years of the SMART protein domain annotation
529 resource. Nucleic Acids Res.
530 72. Schindelin, J., Arganda-Carreras, I., Frise, E., Kaynig, V., Longair, M., Pietzsch, T.,
531 Preibisch, S., Rueden, C., Saalfeld, S., Schmid, B., et al. (2012). Fiji: an open-source platform for
532 biological-image analysis. Nat Methods *9*, 676-682.
533

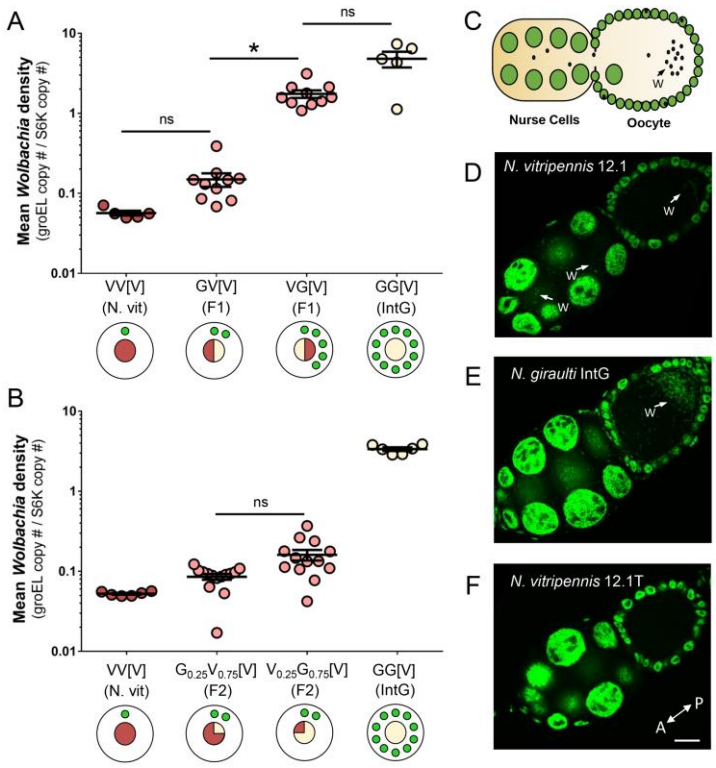

Figure 1. Disparities in *w*VitA titers begin during oogenesis and are established through a maternal genetic effect.

(A) *w*VitA densities in female pupae from parental *N. vitripennis*, *N. girault* IntG, and their reciprocal F1 hybrids.

(B) *w*VitA densities in F2 pupae from F1 females backcrossed to their paternal line. For each cross, genotype (male x female) is followed by cytotype in brackets (V = *N. vitripennis*, G = *N. girault*, number = estimated proportion of genotype). For the circle diagrams, the inner circle represents the expected percentage of the nuclear genome that is of *N. vitripennis* (red) or *N. girault* (cream) origin. Green circles represent *w*VitA load (not drawn to scale). Error bars represent mean ± S.E.M. *$p < 0.05$, post-hoc Dunn's test.

(C) Diagram of a *Nasonia* egg chamber. Large green circles represent host nuclei and small black circles represent *Wolbachia.*

(D) Stage 3 egg chambers with host and *Wolbachia* DNA stained with SYTOX Green from *w*VitA-infected *N. vitripennis*.

(E) Stage 3 egg chambers with host and *Wolbachia* DNA stained with SYTOX Green from *w*VitA-infected *N. giraulti* IntG.

(F) Stage 3 egg chambers with host and *Wolbachia* DNA stained with SYTOX Green from uninfected *N. vitripennis*. Examples of *Wolbachia* cells are labeled with a "W" and white arrows. A = anterior, P = posterior, Scale bar = 15 μm.

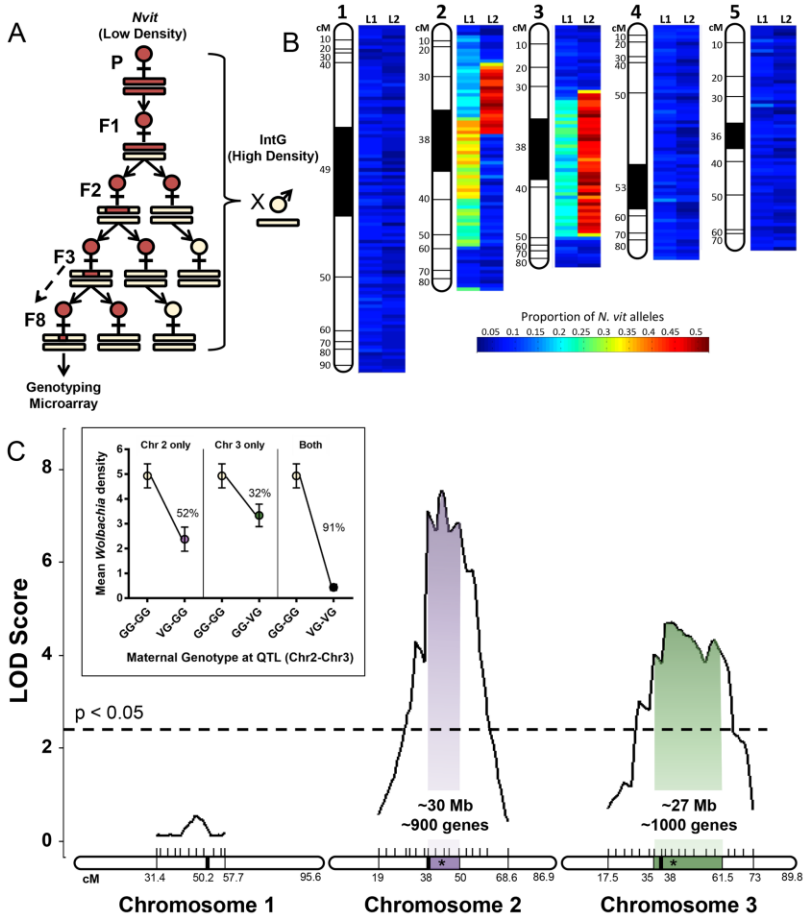

Figure 2. Two genomic regions interact additively to suppress *w*VitA titers.

(A) Schematic of introgression using density phenotype (red female = low, cream female = high) as proxy for maternal genotype (red bar = *N. vitripennis*, cream bar = *N. giraulti*). Eighth generation females with lowest embryonic *Wolbachia* densities were genotyped on a *Nasonia* microarray.

(B) Heatmap of the proportion of *N. vitripennis* alleles across the genome in a pool of three females from each introgression line (L1 or L2). The proportion of *N. vitripennis* alleles is scaled from 0 to 0.5, where 0 = no *N. vitripennis* alleles and 0.5 = all females were heterozygous. Areas were considered enriched for *N. vitripennis* alleles at ≥ 0.2.

584 (C) Plot of LOD score after QTL mapping of F2 females. Shaded regions represent the 95% Bayes
585 credible interval for significant QTL peaks (star). Dashed line represents genome-wide
586 significance threshold at $\alpha = 0.05$.
587 (C, inset) *Wolbachia* density (mean ± S.E.M) of offspring based on maternal genotype at each
588 QTL peak (V = *N. vitripennis*, G = *N. giraulti*). Percent reduction in densities is compared to
589 offspring of F2 homozygous *N. giraulti* females. All maps are based on the *Nasonia* genetic map
590 [50].
591 See also Table S1.
592
593
594
595
596
597
598
599
600
601
602
603
604
605
606
607
608
609
610

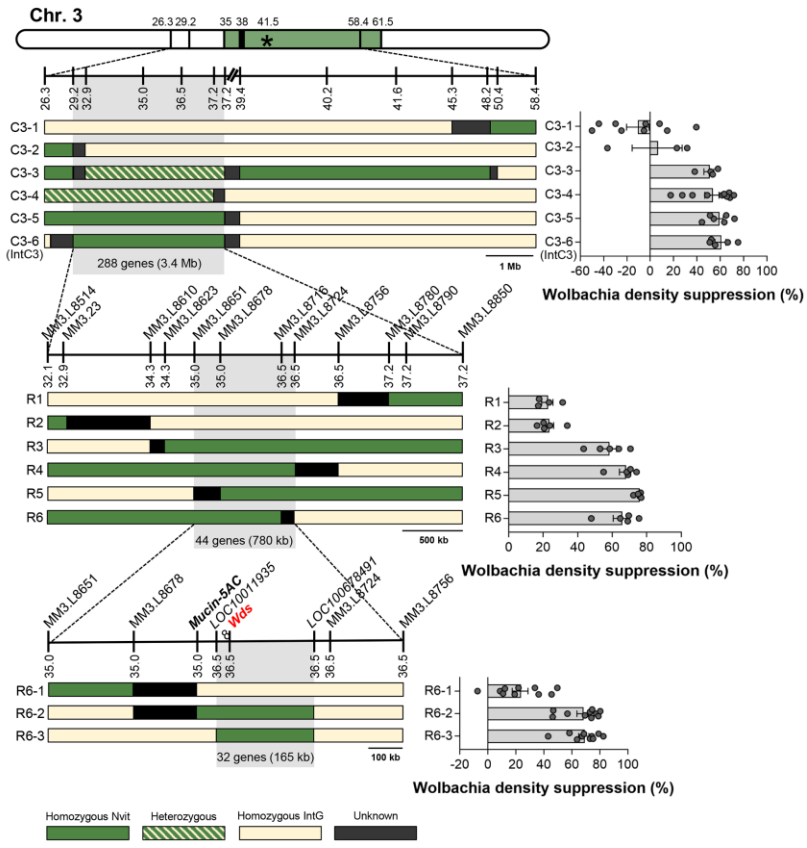

Figure 3. Segmental introgression lines narrow the chromosome 3 candidate region to 32 genes.

Diploid genotypes are depicted as haplotypes, where green bars represent *N. vitripennis* homozygous regions, dashed bars are heterozygous regions, solid cream bars are *N. girault*i IntG homozygous regions, and black bars are recombination breakpoints between two markers. The star and colored region on the chromosome map represent the QTL peak and 95% Bayes credible interval, respectively. Line graphs represent chromosome length in Mb and are drawn to scale except for centromeric regions (broken dashes at top of the figure). Names of the molecular markers (MM) used for genotyping (see Table S1) are provided above the line graphs, and their locations in cM based on the genetic map from [50] are located below the line graphs. The bar graphs show the mean percent effect on density suppression in pupal offspring from all individual

623 mothers with the same haplotype. Error bars denote mean ± S.E.M. See also Table S1 and Table
624 S3.
625
626
627
628
629
630
631
632
633
634
635
636
637
638
639
640
641
642
643
644
645

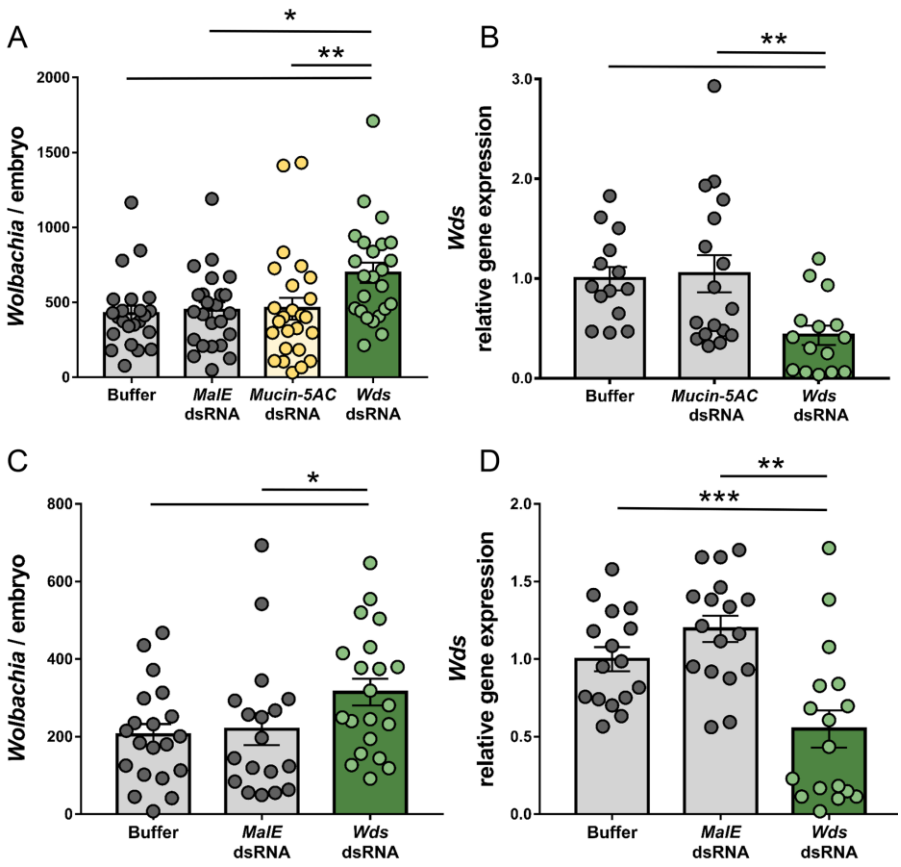

Figure 4. The *N. vitripennis* allele of *Wds* suppresses densities of vertically-transmitted *Wolbachia*.

(A) Number of *w*VitA *Wolbachia* per embryo from IntC3 females that were buffer-injected, injected with dsRNA against control genes *MalE* or *Mucin-5AC*, or injected with dsRNA against Wds_V. *p < 0.05 and **p < 0.01 post-hoc Dunn's multiple comparisons test.

(B) Relative gene expression of Wds_V in late pupae of *Wds*-RNAi and *Mucin-5AC*-RNAi females normalized to Wds_V expression in buffer-injected females. **p<0.01, Mann-Whitney U test.

(C) Number of *w*VitA *Wolbachia* per embryo from R6-3 females that were buffer-injected, injected with dsRNA against control gene *MalE* or injected with dsRNA against Wds_V. *p < 0.05, Mann-Whitney U test.

(D) Relative gene expression of Wds_v in late pupae of *Wds*-RNAi and *MalE*-RNAi females normalized to Wds_v expression in buffer-injected females. **p<0.01, ***p < 0.001, Mann-Whitney U test. All error bars represent mean ± S.E.M.

See also Figure S1, Figure S2, Table S2, and Table S3.

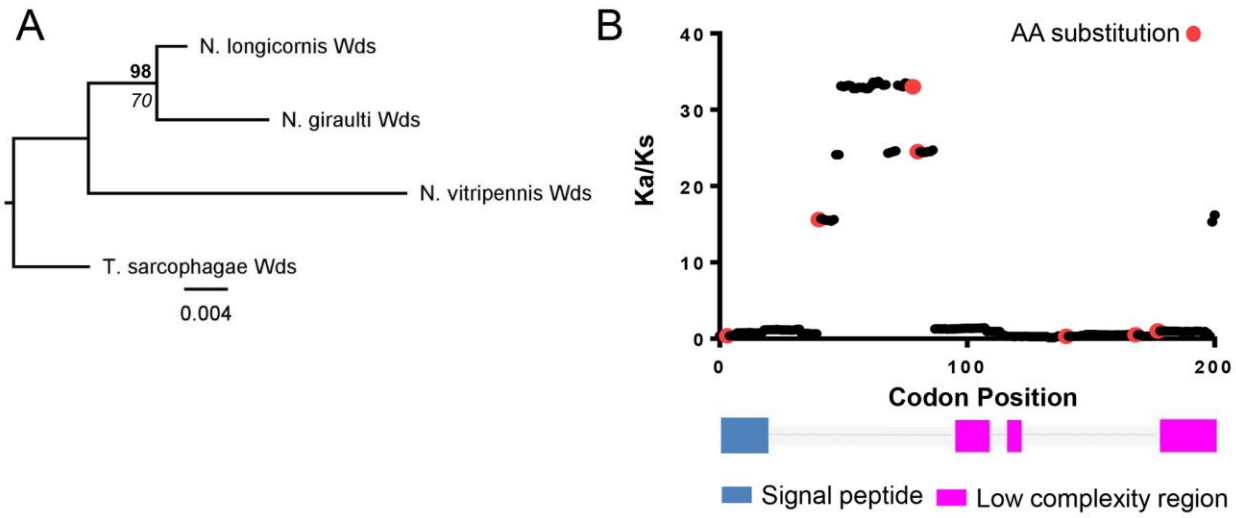

680

681 **Figure 5. The *N. vitripennis* allele of *Wds* is under positive selection.**

682 (A) Amino acid phylogeny of Wds across the *Nasonia* genus and *Trichomalopsis sarcophagae*.

683 Bold text above branch denotes Bayesian posterior probability. Italic text below branch denotes

684 maximum likelihood bootstrap value. Scale bar denotes amino acid substitutions per site.

685 (B) Plot of Ka/Ks ratios based on a sliding window analysis across the *N. vitripennis* and *N.*

686 *giraulti Wds* coding sequences. Red circles indicate the locations of the seven amino acid

687 substitutions unique to *N. vitripennis* Wds. Diagram below illustrates location of the predicted

688 signal peptide and low complexity regions of the Wds protein.

689 See also Figure S3 and Table S4.

690

STAR METHODS

Contact for Reagent and Resource Sharing

Further information and requests for resources and reagents should be directed to and will be fulfilled by the Lead Contact, Seth R. Bordenstein (s.bordenstein@vanderbilt.edu).

Experimental Model and Subject Details

Nasonia Parasitoid Wasps

Experiments were performed with *Nasonia vitripennis* strain 12.1, *N. giraulti* strain IntG12.1 or hybrids of these two species. *N. vitripennis* 12.1 is singly-infected with native *Wolbachia* strain *w*VitA and was derived from the double-infected *N. vitripennis* R511 (*w*VitA and *w*VitB) after a prolonged period of diapause [36]. *N. giraulti* strain IntG12.1 was generated by backcrossing *N. vitripennis* 12.1 females to uninfected *N. giraulti* Rv2x(u) males for nine generation [47], producing hybrids with an *N. giraulti* genome and an *N. vitripennis* cytoplasm harboring *w*VitA. All *Nasonia* were reared at 25°C in constant light on *Sarcophaga bullata* fly hosts reared in house on bovine liver from Walnut Hills Farm.

Method Details

Quantitative analysis of *Wolbachia* densities

Genomic DNA was extracted from pupae or adult *Nasonia* using the Gentra Puregene Tissue Kit (Qiagen) according to the manufacturer's protocol. Real-time quantitative PCR (qPCR) was performed on a CFX96 Real-Time system (Bio-Rad) using a total reaction volume of 25 µl: 12.5 µl of iQ SYBR Green Supermix (Bio-Rad), 8.5 µl of sterile water, 1.0 µl each of 5 µM forward and reverse primers, and 2 µl of target DNA in single wells of a 96-well plate (Bio-Rad). All qPCR

reactions were performed in technical duplicates and included a melt curve analysis to check for primer dimers and nonspecific amplification. Selective amplification was performed using primers previously described for the *Wolbachia groEL* gene [62] and *Nasonia NvS6K* gene [63]. Standard curves for each gene were constructed as previously described [63] using a log10 dilution series of larger PCR products of known concentrations for each gene. *groEL* and *S6K* copy numbers for each sample were calculated based on the following standard curve equations: *groEL*: y = -3.367x + 35.803 and *S6K:* y = -3.455x + 35.908, where y = averaged Ct value between technical duplicates and x = log starting quantity of template DNA. *Wolbachia* density was calculated by dividing *groEL* copy number by *S6K* copy number for each sample. Since diploid female *Nasonia* have twice the number of *S6K* copies than males, all experiments comparing *Wolbachia* densities were performed on either all male or all female samples to eliminate *S6K* copy number as a confounding factor in the statistical analyses.

Microsatellite marker genotyping

Primers used to amplify microsatellite markers that differ in size between *N. vitripennis* and *N. giraulti* are listed in Table S1. Microsatellite markers not previously published were identified by aligning *N. vitripennis* and *N. giraulti* genomic sequences using the Geneious alignment tool in Geneious Pro v5.5.8 (Biomatters). The Geneious primer design tool was then used to generate primer sets spanning each microsatellite. All PCR reactions were run on a Veriti Thermal Cycler (Applied Biosystems) with a total reaction volume of 15 µl: 7.5 µl of GoTaq Green Master Mix (Promega), 3.6 µl of sterile water, 1.2 µl of 5µM forward and reverse primers (see Table S1 for annealing temp.), and 1.5 µl of target DNA. PCR products were run on 4% agarose gels in TBE buffer (Sigma) at 90 volts for 2.5 to 6 hours, stained with GelRed (Biotium) according to

737 manufacturer's protocol, and imaged on a Red Personal Gel Imager (Alpha Innotech). New
738 markers were validated based on predicted band size using *N. vitripennis* 12.1 and *N. giraulti* IntG
739 as controls.
740
741 Phenotype-based selection and introgression coupled with a genotyping microarray
742 *N. vitripennis* females (low *w*VitA density) were backcrossed with *N. giraulti* IntG males
743 (high *w*VitA density) for nine generations. For each generation of backcrossing, five female pupal
744 offspring were pooled from each hybrid mother, and the pupal *Wolbachia* densities were measured
745 using qPCR. Sisters of the pupae with the lowest *Wolbachia* densities were then used as mothers
746 in the next round of backcrossing. Two independent selection lines were maintained
747 simultaneously along with control lines of pure-breeding *N. vitripennis* and *N. giraulti*. After eight
748 generations of selection, the three females from each introgression line that produced ninth-
749 generation offspring with the lowest *Wolbachia* densities were pooled and their DNA extracted
750 using the DNeasy Blood and Tissue Kit (Qiagen) with the protocol for purification of DNA from
751 insects. To obtain enough DNA for microarray hybridization, we used the REPLI-g Mini Kit
752 (Qiagen) with the protocol for 5 µl of DNA template to amplify genomic DNA overnight at 30 °C,
753 then purified the DNA using ethanol precipitation. The final concentration for each sample was
754 diluted to 1 µg/µl and a total of 10 µl was sent to The Center for Genomics and Bioinformatics at
755 Indiana University to be processed on a *Nasonia* genotyping microarray (Roche NimbleGen) tiled
756 with probes for 19,681 single nucleotide polymorphisms and indels that differ between *N.*
757 *vitripennis* and *N. giraulti* [50].
758 For each sample, the proportion of *N. vitripennis* alleles at each marker was determined based
759 on the ratio of hybridization to the *N. vitripennis*-specific probe versus hybridization to the *N.*

760 *girault*i-specific probe, as previously described [50]. To verify species-specificity of these markers
761 for our *Nasonia* strains, we also genotyped *N. vitripennis* 12.1 and *N. girault*i IntG control females
762 on the array, and markers that did not display the correct specificity within one standard deviation
763 of the median were removed from subsequent analyses (5,301 markers total). The remaining
764 markers were then manually mapped back to the most recent *Nasonia* linkage map [50]. Since all
765 introgression females received one copy of their diploid genome from their *N. girault*i father, the
766 theoretical maximum proportion of *N. vitripennis* alleles at each marker cluster for experimental
767 samples is 0.5. The proportion of *N. vitripennis* alleles was averaged for every 22 consecutive
768 markers across each chromosome, and heat maps were generated using the HeatMap function in
769 MATLAB (MathWorks).
770
771 QTL Analysis
772 F2 hybrid females (N = 191) were generated by backcrossing F1 *N. vitripennis*/*N. girault*i
773 hybrids to *N. girault*i IntG males. F2 females were then backcrossed again to *N. girault*i IntG and
774 allowed to lay offspring. Five female pupae from each F2 female were pooled and their *Wolbachia*
775 densities measured using qPCR. Females that produced offspring with densities within the highest
776 and lowest quartile of the density distribution (N = 42 for each quartile) were selectively genotyped
777 with 47 microsatellite markers spread across chromosomes 1, 2 and 3 with an average distance of
778 3 cM between markers. Phenotypic information for all 191 F2 females was included in the mapping
779 analyses to prevent inflation of QTL effects due to the biased selection of extreme phenotypes
780 [51]. QTL analyses were performed in R (version 3.0.2) with package R/qtl [64]. Significance
781 thresholds for our dataset were calculated by using a stratified permutation test with the scanone
782 function (1000 permutations). To identify significant QTL and their interactions, we first

783 conducted a one-dimensional, one-QTL scan and a two-dimensional, two-QTL scan using the EM
784 algorithm with a step size of 1 cM and an assumed genotype error probability of 0.001. Two
785 significant QTLs were identified, one each on chromosomes 2 and 3, which were predicted to act
786 additively. The positions of identified QTL were then refined using multiple QTL modeling with
787 the multiple imputation algorithm (200 imputations, step size = 1 cM) assuming a model with two
788 additive QTLs. 95% Bayes credible intervals were calculated for each QTL after multiple QTL
789 modeling using the bayesint function.
790
791 Marker-assisted segmental introgressions
792 Marker-assisted segmental introgression lines were generated by repeatedly backcrossing
793 hybrid females to *N. giraulti* males for nine generations while selecting for *N. vitripennis* alleles
794 at three microsatellite markers on chromosome 3 (MM3.17, NvC3-18, and MM3.37). After the
795 ninth generation, families that maintained an *N. vitripennis* allele at one or more of these markers
796 were selected, and siblings were mated to each other to produce lines containing homozygous *N.*
797 *vitripennis* regions at and around the markers. Individual adult females from each segmental line
798 were genotyped and phenotyped separately (N = 10 – 15 females per line). Females were hosted
799 as virgins, five male pupal offspring per female were pooled, and pupal *Wolbachia* densities were
800 measured using qPCR. Variation across plates for a single experiment was reduced by including a
801 set of parental DNA controls on all plates. The parental fold-change was then calculated by
802 dividing the average *N. giraulti* control density by the average *N. vitripennis* control density. To
803 calculate the sample fold-change, the absolute density for each sample was divided by the average
804 density of the *N. vitripennis* control. To determine how "effective" each segmental introgression

line was at reducing densities, we calculated the percent effect on density suppression for each sample using the following equation:

$$\%\ effect\ \ on\ density\ suppresion = \left(1 - \frac{sample\ fold\ change}{parental\ fold\ change}\right) \times 100$$

Each female was genotyped with markers across the region of interest, all females with identical genotypes across all markers were grouped together, and their percent effects on density suppression were averaged.

For the two subsequent rounds of introgression lines (R1 to R10 and R6-1 to R6-3), 300 IntC3 line females or 800 R6 line virgin females, respectively, were backcrossed to IntG males. The resulting virgin F1 females produced haploid, recombinant males. These recombinant males were mated to IntG females to produce heterozygous female offspring with the recombinant genotype. Siblings were then mated to each other and genotyped for two more generations to produce recombinant lines containing homozygous *N. vitripennis* introgressed regions reduced in size.

A subset of the genes within the 32-gene candidate region were genotyped using sequencing primers (Table S5) to amplify PCR products 250-750 bp for each of the R6 recombinant lines (R6-1 to R6-3) for Sanger sequencing (GENEWIZ). All PCR reactions were run on a Veriti Thermal Cycler (Applied Biosystems) with a total reaction volume of 15 µl: 7.5 µl of GoTaq Green Master Mix (Promega), 3.6 µl of sterile water, 1.2 µl of 5µM forward and reverse primers (see Table S5 for annealing temp.), and 1.5 µl of target DNA and purified using the QIAquick PCR Purification kit (Qiagen). At least 6 distinct single nucleotide polymorphisms (SNPs) between *N. vitripennis* and *N. giraulti* alleles were used to characterize the allele for each recombinant line using Geneious Pro v5.5.8 (Biomatters).

828

829 RNA-seq of ovaries

830 One-day old females from *Nasonia* strains *N. vitripennis* 12.1, *N. giraulti* IntG, and *N.*
831 *vitripennis/N. giraulti* introgression line IntC3 were hosted as virgins on *S. bullata* pupae for 48
832 hours to stimulate feeding and oogenesis. Females were then dissected in RNase-free 1X PBS
833 buffer, and their ovaries were immediately transferred to RNase-free Eppendorf tubes in liquid
834 nitrogen. Forty ovaries were pooled for each replicate and 4-5 biological replicates were collected
835 per *Nasonia* strain. Ovaries were manually homogenized with RNase-free pestles, and their RNA
836 was extracted using the Nucleospin RNA/Protein Kit (Macherey-Nagel) according to the
837 manufacturer's protocol for purification of total RNA from animal tissues. After RNA purification,
838 samples were treated with RQ1 RNase-free DNase (Promega) for 1 hour at 37 °C, followed by an
839 ethanol precipitation with 1/10th volume 3M sodium acetate and 3 volumes 100% ethanol
840 incubated overnight at -20 °C. PCR of samples with *Nasonia* primers NvS6KQTF4 and
841 NVS6KQTR4 [63] revealed some residual DNA contamination, so DNase treatment and ethanol
842 precipitation were repeated. After the second DNase treatment, PCR with the same primer set
843 confirmed absence of contaminating DNA. Sample RNA concentrations were measured with a
844 Qubit 2.0 Fluorometer (Life Technologies) using the RNA HS Assay kit (Life Technologies). All
845 samples were run multiplexed on two lanes of the Illumina HiSeq3000 (paired-end, 150 bp reads,
846 ~30M reads) at Vanderbilt's VANTAGE sequencing core. Raw reads were trimmed and mapped
847 to the *N. vitripennis* genome Nvit_2.1 (GCF_000002325.3) in CLC Genomics Workbench 8.5.1,
848 allowing ten gene hits per read using a minimum length fraction of 0.9 and a minimum similarity
849 fraction of 0.9. The number of reads generated for each sample and the percentage of reads that
850 mapped to the *N. vitripennis* genic and intergenic regions are provided in Table S2. Significant

851 differential gene expression was determined in CLC Genomics Workbench 8.5.1 at $\alpha = 0.05$ for
852 unique gene reads using the Empirical analysis of DGE tool, which is based on the edgeR program
853 commonly used for gene expression analyses [65].
854
855 RT-qPCR validation of RNA-seq results
856 One-day old females from *N. vitripennis* 12.1, *N. giraulti* IntG, and IntC3 were hosted with
857 two *S. bullata* pupae and honey to encourage ovary development. After 48 hours, ovaries were
858 removed in RNase-free PBS, flash-frozen in liquid nitrogen then stored at -80 ˚C. 4-5 replicates of
859 fifty ovaries per replicate were collected for each *Nasonia* strain. Total RNA was extracted from
860 each sample using Trizol reagent (Invitrogen) with the Direct-zol RNA Miniprep kit (Zymo
861 Research) then treated with the DNA-free DNA Removal kit (Ambion) for one hour at 37 ˚C. After
862 ensuring with PCR that all DNA had been removed, RNA was converted to cDNA using the
863 SuperScript VILO cDNA Synthesis kit (Invitrogen).
864 RT-qPCR was performed on a CFX96 Real-Time system (Bio-Rad) using a total reaction
865 volume of 25 µl: 12.5 µl of iTaq Universal SYBR Green Supermix (Bio-Rad), 8.5 µl of sterile
866 water, 1 µl each of 5 µM forward and reverse primers (see STAR Methods), and 2 µl of target
867 cDNA in single wells of a 96-well plate (Bio-Rad). All RT-qPCR reactions were performed in
868 technical duplicates and included a melt curve analysis to check for nonspecific amplification. The
869 60S ribosomal protein L32 (also known as RP49) was used as an expression control. All primers
870 for RT-qPCR are provided in the STAR Methods. Expression values for each candidate gene were
871 calculated using the $\Delta\Delta C_t$ method of relative quantification [66] with RP49 as the reference gene.
872 Fold-change was determined by normalizing expression values to the mean expression value of *N.*
873 *giraulti* IntG for each gene.

874

875 RNAi of candidate genes

876 To generate DNA template for dsRNA synthesis, primers with a T7 promoter sequence on
877 the 5' end of each primer were used to amplify a 450-700 bp region of the targeted genes (see
878 STAR Methods) by PCR using *N. vitripennis* whole-body cDNA as template. PCR amplicons were
879 separated by electrophoresis on a 1% agarose gel, excised, and purified using the QIAquick Gel
880 Extraction kit (Qiagen). The purified PCR products were used as template for a second PCR
881 reaction with the same gene-specific T7 primers, then purified using the QIAquick PCR
882 Purification kit (Qiagen). After quantification with the Qubit dsDNA Broad Range Assay kit
883 (Thermo Fisher Scientific), approximately 1 ug of the purified PCR amplicon was used as template
884 for dsRNA synthesis with the MEGAScript RNAi kit (Ambion). The dsRNA synthesis reaction
885 was incubated for six hours at 37 ˚C, treated with RNase and DNase for one hour at 37 ˚C, then
886 column-purified according to the manufacturer's protocol.

887 For injection, the dsRNA was used at a final concentration standardized to 750 ng/ul dsRNA.
888 A Nanoject II (Drummond Scientific) was used to inject 23 nl of dsRNA (or MEGAScript kit
889 elution buffer) into the ventral abdomen of female *Nasonia* at the yellow pupal stage. After
890 emerging as adults, injected females were given honey and hosted individually on two *S. bullata*
891 pupae for 48 hours. On the third day after emergence, they were transferred to new vials where
892 they were presented with a single *S. bullata* host. After five hours, the hosts were opened and up
893 to ten embryos were collected in a 1.5 ml Eppendorf tube for each female and stored at -80 ˚C.
894 The females were given two hosts overnight, and then the same process was repeated again on the
895 fourth day.

The number of *Wolbachia* cells per embryo from injected females three and four days post emergence was determined using qPCR with *Wolbachia groEL* primers as described above. *Wolbachia* titers were not normalized to *Nasonia* gene copy number because early embryos have varying numbers of genome copies depending on how many rounds of mitotic division they have undergone [67]. To determine the knock-down efficiency of each dsRNA injection, RNA extraction and RT-qPCR of black pupae, five days post injection, were performed with 14-17 biological replicates from each treatment group as described above using the gene-specific qPCR primers in the STAR Methods.

Wds evolution and domain analyses

N. giraulti and *N. longicornis* nucleotide sequences of *Wds* were obtained from NCBI genomic scaffold sequences GL276173 and GL277955, respectively, and indels were manually extracted in Geneious Pro v11.0.3 (Biomatters) based on homology to *N. vitripennis* gene LOC1006079092. Protein alignment of Wds amino acid sequences for the three *Nasonia spp.* and its homolog in *T. sarcophagae* (TSAR_005991) was performed using the Geneious alignment tool. MEGA7.0.26 [68] was used to identify the JTT model as the best model of protein evolution for the alignment based on corrected Akaike information criterion (AICc). PhyML [69] and MrBayes [70] were executed in Geneious with default parameters to construct a maximum likelihood tree with bootstrapping and a Bayesian tree with a burn-in of 100,000, respectively.

To identify residues under positive selection in Wds, Ka/Ks values were calculated based on a pairwise alignment of the *N. vitripennis* and *N. giraulti Wds* coding sequences using a sliding window analysis (window = 30 AA, step size = 1 AA, Standard Code for genetic code input) in the SWAKK bioinformatics web server [59]. Analysis of Wds for protein structures and conserved

919 domains was performed using the SMART online software at http://smart.embl-heidelberg.de
920 [71]. Protein pIs were predicted using the online ExPASY Compute pI/Mw tool.
921
922 Staining *Wolbachia* in *Nasonia* ovaries
923 Female *Nasonia* were hosted on *Sarcophaga bullata* pupae for two to three days before
924 dissection to encourage ovary development. For nuclear staining of ovaries, females were
925 dissected in 1X phosphate-buffered saline (PBS) solution, where ovaries were removed with
926 forceps and individual ovarioles were separated with fine needles. Ovaries were fixed in 4%
927 formaldehyde in PBS with 0.2% Triton X-100 (PBST) for 20 minutes at room temperature then
928 transferred to a 1.5 ml Eppendorf tube containing PBST. Samples were washed quickly three times
929 with PBST then incubated in PBST plus 1 mg/ml RNase A for three hours at room temperature
930 then overnight at 4 ˚C. After removing the RNase A solution, ovaries were incubated at room
931 temperature for 15 minutes in PBST with 1:300 SYTOX green nucleic acid stain (Thermo Fisher
932 Scientific) before washing twice with PBST, 15 minutes each time. Ovaries were then transferred
933 to a glass slide and mounted in ProLong Gold antifade solution (Thermo Fisher Scientific) and
934 covered with a glass cover slip sealed with nail polish.
935 All images were acquired on a Zeiss LSM 510 META inverted confocal microscope at the
936 Vanderbilt University Medical Center Cell Imaging Shared Resource core and processed with Fiji
937 software [72].
938
939 **Quantification and Statistical Analyses**
940 All statistical analyses, unless otherwise noted, were performed in GraphPad Prism 6.07
941 (GraphPad Software, La Jolla, CA). Outliers were removed from the results on embryonic

Wolbachia titers and *Wds* RT-qPCR using the ROUT method, Q=1%. Non-parametric tests were used on all data since most data did not pass a Shapiro-Wilk test for normality or sample sizes were too small. Mann-Whitney U tests were used for comparisons between two groups, whereas a Kruskal-Wallis test was used to compare multiple groups. If the Kruskal-Wallis test was significant ($p \leq 0.05$), a post-hoc Dunn's test of multiple comparisons was used to calculate significance for all pair-wise combinations within the group. All averages are reported as mean ± S.E.M. For all quantifications of pupal *Wolbachia* densities, sample size "N" represents one pool of five pupae. For any data referring to adult *Nasonia* (genotyping, RNAi or RT-qPCR), sample size "N" denotes individual *Nasonia*.

Data and Software Availability

RNA-seq data generated in this study will be available in the Sequence Reads Archive.

SUPPLEMENTAL INFORMATION

Supplemental Information includes three figures, five tables and two datasets.

Data S1. QTL genotypes and phenotypes, Related to Figure 2.

V/G = heterozygous female (red), G/G = homozygous *N. girault*i female (cream), and question marks indicate an unknown genotype. Markers that fall within the 95% Bayes credible interval are highlighted in purple (chromosome two) or green (chromosome three).

Data S2. Chromosome 3 segmental introgression haplotypes and their effects on *w*VitA density suppression, Related to Figure 3.

cM locations based on genetic linkage map from [50].